Small Satellite Operational Phase Thermal Analysis and Design: A Comparative Study

Ahmed ELWETEEDY[1], Ali ELMAIHY*,[1], Ahmed ELHEFNAWY[2]

*Corresponding author
[1]Department of Mechanical Power and Energy, Military Technical College,
Kobry El koba, Cairo, Egypt,
ali.elmaihy@mtc.edu.eg*
[2]Space Technology Center,
Kobry El koba, Cairo, Egypt

DOI: 10.13111/2066-8201.2021.13.4.6

Received: 02 July 2021/ Accepted: 17 November 2021/ Published: December 2021

Abstract: *This paper is about the modeling and design of the passive thermal control system for the European Student Earth Orbiter (ESEO) satellite. A detailed thermal model was created in Thermal Desktop software. The model was running for the operative phase which includes cycles of 28 orbits. During these 28 orbits, there are several modes (10 modes). Each mode has a specific duration, attitude (Sun-nadir), and certain internal heat dissipation. The design of the passive thermal control system was based on controlling the conductive and radiative heat exchange between the internal components and the mounting panels, between panels themselves, and controlling external radiation exchange to achieve the desired components temperature ranges. The temperature results from simulations were presented to show the expected component temperatures and to demonstrate that the passive thermal control system met the requirements of the temperature limits. The final passive thermal control design shows that the satellite components temperatures were always maintained within their required limits during the operational phase.*

Key Words: *Aerospace Engineering, satellite thermal control, modeling*

1. INTRODUCTION

Due to their lower weights and smaller sizes, small satellites are more attractive than conventional satellites. They reduce costs because they require smaller and cheaper launch vehicles and multiple satellite can be carried in in one launch vehicle. Components in small satellites are densely packed resulting in the dissipation of internally generated heat that becomes more critical and considerable care must be used in the design of a satellite thermal control system (TCS) [1–3]. It plays a primary role in determining the final satelliteconfiguration, components locations, orbital parameters, attitude, and power requirements [4].

For the thermal control system to be successful, accurate thermal modeling must be performed throughout the design, testing, and all phases of operation of the satellite. The passive thermal control systems do not require any mechanical moving parts or moving fluids but usually comprise specially selected surface coatings (paints and tapes) that control internal and external radiation heat exchange, as well as conductive elements and gaskets to thermally

couple or de-couple satellite components as required [5, 6] to delimit the range of temperatures to which the different components will be exposed. For simplicity and to conserve power, small satellite thermal control systems are often designed to be passive. They have also other advantages in terms of reliability and cost and no power consumption.

Conducting an assessment of the thermal behavior of a small satellite by analytical solutions can only be found for simple geometric scenarios that that are often not representative of real satellite design situations [7]. So, recent complex numerical algorithms [8, 9] were developed. These algorithms require the implementation of a complex numerical simulation. These simulations solve the governing differential equations numerically by discretization of the differential equation over the solution domain which is represented by a set of nodes. The solution is carried out under a specified set of boundary conditions. The discretization techniques are either finite-difference time-domain (FDTD), finite element (FEM), or moments (MoM) methods. Thermal analysis commercial software committed to spacecraft permits the conversion from comprehensive to condensed thermal mathematical models [4]. Different commercial software programs are used in literature for passive and active thermal control of small satellites. Table 1 summarizes some examples for passive thermal control system for small satellites.

Table 1. Examples of small satellite passive TCS

No	Satellite name	Country	Year	Software used	Ref.
1	Compass-1	Germany	2003	ANSYS	[10]
2	A cubesat	USA	2009	Thermal Desktop	[11]
3	Turksat-3U	Turkey	2010	Therm-XL	[12]
4	OSIRIS-3U	USA	2012	COMSOL	[13]
5	CanX-4	Canada	2014	Siemens' NX 8	[5, 14]
6	QARMAN	Belgium	2015	ESATAN	[15]
7	Delffi	Netherlands	2015	ESATAN	[16]
8	MR sat- MRS sat	USA	2018	Thermal Desktop	[17]

Sometimes passive thermal control system does not meet the requirements to maintain the temperature of the components within their limits such as AlSat 1B [18]. So, in critical locations, an external control (active control system) is demanded [19] such as a heater. The disadvantage of using an active control system is that it requires complex designs and additional electrical power and costs. Table 2 summarizes some examples of the active thermal control systems.

Table 2. Examples of small satellite active TCS

No	Satellite name	Country	Year	Software used	Ref.
1	OUFTI-1	Belgium	2008	ESATAN	[20]
2	ESEO	Italy	2012	ESATAN	[21]
3	Amazonia-1	Brazil	2014	Thermal Desktop	[22]
4	canX-7	Canada	2014	Siemens' NX 8	[23]
5	MIST	Sweden	2017	Thermica	[24]

An active TCS satellite example is the European Student Earth Orbiter "ESEO" satellite. This satellite is a mission created by the education satellite program of the European Space Agency. The mission was based on a Sun-synchronous orbit with an altitude of 520km, an inclination of 97.48°, and Local Time of Ascending Node (LTAN) 10:30. The modeling of the thermal control system was carried out in two phases with different software. In the first phase, MiniTAN software was used to model the thermal behavior of the satellite thermal behavior. Unfortunately, MiniTAN is restricted to a 50 node model and does not incorporate a3d graphic

interface. So, in the second phase thermal control design, a more accurate model solution was made by using ESATAN [21]. The new model used 176 nodes instead of 50 nodes in the former model. The radiative heat interchange was calculated among satellite components and so the external heat fluxes. Results and various analyses carried out lead to the conclusion that an active thermal subsystem must be used. The main objective of this work is summarized in the following question: Is it possible for ESEO satellite to be controlled by passive means? A detailed passive thermal model for the operational phase was created in Thermal Desktop software [25]. The model results were compared with ESEO published results.

2. ESOE OPERATIONAL PHASE DESCRIPTION

Fig. 1 shows the internal views for the satellite under investigation. The satellite is a cuboid shape with six structural panels, two deployable and one fixed solar panel. Its dimensions are 967 × 750 × 680 mm and its mass is less than 100 kg. The mission was based on Sun-synchronous orbit with an elevation of 520 km and an inclination of 97.48° with Local Time of Ascending Node (LTAN) 10:30.

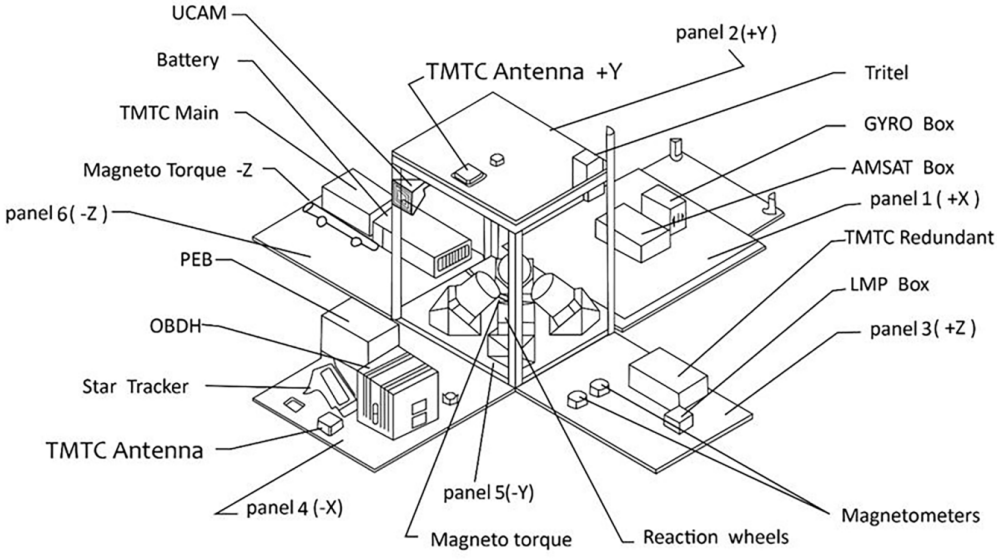

Fig. 1 Internal view of ESEO satellite adapted from [21]

The ESEO has five main phases: launch and early operations phase; operational phase; extended phase; post-mission phase and satellite disposal. The operational phase is the main concern of this study. After the launch and early operation phase, the satellite starts its normal operation phase to achieve the mission objectives and uses the payloads for six months. According to the mission objectives, the spacecraft operates the following payloads Tridimensional Telescope dosimeter (TriTel-S), Micro camera (uCAM), Langmuir plasma diagnostic probe (LMP), the Radio Amateur Satellite Corporation (AMSAT) system, Reaction Wheel, and Star Tracker.

The operative phase is divided into cycles of 28 orbits. During these 28 orbits, there are several modes (10 modes) and each mode has a specific duration, attitude (Sun-nadir), and certain internal heat dissipation. Thus, each component will have a different heat dissipation and it is important to define the heat dissipation for every component in all modes. For the ESEO mission, there are two pointing directions, Sun and nadir pointing. In Sun pointing, the

x-axis tracks the Sun and the y-axis pointing to the north celestial pole, and in nadir pointing, the -z-axis points to the earth and the y-axis follows the velocity vector. The satellite is mostly in the Sun pointing orientation. The nadir pointing orientation only occurs in three modes (3,4 and 10) to point the UCAM towards the earth for shooting. Table 3 presents the 28 orbits operative phase modes. The different modes (10 modes) are given in Table 4. Both tables are recreated from [21]. A summary of the internal heat dissipation of each piece of equipment for all operating modes is given in Table 5.

Table 3 Twenty-eight orbits operational phase modes

Orbit No	Mode Sequence	Attitude	Time [min]	Dissipated Power[W]	Orbits (total)	Mode Sequence	Attitude	Time [min]	Dissipated Power[W]
0.63	Mode 1	Sun	60.00	100.42	15.00	Mode 5	Sun	95.00	117.94
0.84	Mode 6	Sun	20.00	105.22					
1.00	Mode 1	Sun	15.00	100.42					
1.11	Mode 7	Sun	10.00	103.72	16.00	Mode 1	Sun	95.00	100.42
2.00	Mode 1	Sun	85.00	100.42					
2.55	Mode 1	Sun	52.67	100.42	16.11	Mode 7	Sun	10.00	103.72
2.63	Mode 2	Sun	7.33	122.02	17.00	Mode 1	Sun	85.00	100.42
2.84	Mode 6	Sun	20.00	105.22					
2.92	Mode 2	Sun	7.33	122.02					
3.00	Mode 1	Sun	7.67	100.42					
3.16	Mode 10	Nadir	15.00	127.54	17.63	Mode 1	Sun	60.00	100.42
3.24	Mode 4	Nadir	7.33	152.74	17.84	Mode 6	Sun	20.00	105.22
3.39	Mode 10	Nadir	15.00	127.54	18.00	Mode 1	Sun	15.00	100.42
3.63	Mode 1	Sun	22.67	100.42					
3.71	Mode 2	Sun	7.33	122.02					
4.00	Mode 1	Sun	27.76	100.42					
4.03	Mode 8	Sun	2.67	155.26	18.16	Mode 10	Nadir	15.00	127.54
4.11	Mode 9	Sun	7.33	176.86	18.24	Mode 4	Nadir	7.33	152.74
4.63	Mode 1	Sun	50.00	100.42	18.39	Mode 10	Nadir	15.00	127.54
4.92	Mode 1	Sun	27.67	100.42	18.63	Mode 1	Sun	22.67	100.42
5.00	Mode 2	Sun	7.33	122.02	18.71	Mode 2	Sun	7.33	122.02
					19.00	Mode 1	Sun	27.67	100.42
6.00	Mode 5	Sun	95.00	117.94	19.03	Mode 8	Sun	2.67	155.26
					19.11	Mode 9	Sun	7.33	176.86
					19.63	Mode 1	Sun	50.00	100.42
					19.92	Mode 1	Sun	27.67	100.42
					20.00	Mode 2	Sun	7.33	122.02
6.03	Mode 8	Sun	2.67	155.26	20.37	Mode 5	Sun	60.00	117.94
6.11	Mode 9	Sun	7.33	176.86	21.00	Mode 5	Sun	35.00	117.94
6.63	Mode 1	Sun	50.00	100.42					
6.92	Mode 1	Sun	27.67	100.42					
7.00	Mode 2	Sun	7.33	122.02					
7.16	Mode 10	Nadir	15.00	127.54	21.37	Mode 10	Sun	60.00	117.94
7.24	Mode 3	Nadir	7.33	131.14	22.00	Mode 5	Sun	35.00	117.94
7.39	Mode 10	Nadir	15.00	127.54					
7.63	Mode 1	Sun	22.67	100.42					
8.00	Mode 1	Sun	35.00	100.42					
8.11	Mode 7	Sun	10.00	103.72	22.63	Mode 1	Sun	60.00	100.42
8.63	Mode 1	Sun	50.00	100.42	23.00	Mode 1	Sun	35.00	100.42
9.00	Mode 1	Sun	35.00	100.42					
9.63	Mode 1	Sun	60.00	100.42	23.63	Mode 1	Sun	60.00	100.42
10.00	Mode 1	Sun	35.00	100.42	24.00	Mode 1	Sun	35.00	100.42
10.63	Mode 1	Sun	60.00	100.42	24.11	Mode 7	Sun	10.00	103.72
11.00	Mode 1	Sun	35.00	100.42	24.63	Mode 1	Sun	50.00	100.42
					25.00	Mode 1	Sun	35.00	100.42
11.55	Mode 1	Sun	52.67	100.42	25.63	Mode 1	Sun	60.00	100.42
11.63	Mode 2	Sun	7.33	122.02	25.84	Mode 6	Sun	20.00	105.22

11.92	Mode 1	Sun	27.67	100.42	26.00	Mode 1	Sun	15.00	100.42
12.00	Mode 2	Sun	7.33	122.02					
12.55	Mode 1	Sun	52.67	100.42	26.16	Mode 10	Nadir	15.00	127.54
12.63	Mode 2	Sun	7.33	122.02	26.24	Mode 4	Nadir	7.33	152.74
12.92	Mode 1	Sun	27.67	100.42	26.39	Mode 10	Nadir	15.00	127.54
13.00	Mode 2	Sun	7.33	122.02	26.63	Mode 1	Sun	22.67	100.42
					26.71	Mode 2	Sun	7.33	122.02
					27.00	Mode 1	Sun	27.67	100.42
13.63	Mode 1	Sun	60.00	100.42	27.03	Mode 8	Sun	2.67	155.26
14.00	Mode 1	Sun	35.00	100.42	27.11	Mode 9	Sun	7.33	176.86
					27.63	Mode 1	Sun	50.00	100.42
					27.92	Mode 1	Sun	27.67	100.42
					28.00	Mode 2	Sun	7.33	122.02

Table 4. ESEO operational phase modes

Mode No	Description	System / Equipment									
		OBDH	EPS	TMTC	ACS	uCAM	TriTel-S	LMP Langmuir Probe	Star Tracker	Reaction Wheel	AMSAT Payload
Mode 1	Nominal Mode RX	Data Memorization	On	RX On	Stand-by	Off	Off	Off	Off	Off	Off
Mode 2	Nominal Mode RXTX			RXTX On	Stand-by						
Mode 3	Nominal Mode-UCAM- RX			RX On	Fine Pointing	On					
Mode 4	Nominal Mode-UCAM- RXTX			RXTX On	Fine Pointing						
Mode 5	Nominal Mode-TriTel-S/LMP- RX			RX On	Stand-by	Off	On	On	On		
Mode 6	Nominal Mode-Star Tracker -RX			RX On	Auxiliary		Off	Off	Off		
Mode 7	Nominal Mode-RW -RX			RX On	Auxiliary					On	
Mode 8	Nominal Mode-AMSAT-RX			RX On	Stand-by					Off	On
Mode 9	Nominal Mode-AMSAT-RXTX	Data Transmission		RXTX On	Stand-by						
Mode 10	Nominal Maneuver-RX	Nominal		RX On	Fine Pointing					Off	Off

Table 5. Heat dissipation of each piece of equipment for all operating modes

Component	Pannel	Mode 1	Mode 2	Mode 3	Mode 4	Mode 5	Mode 6	Mode 7	Mode 8	Mode 9	Mode 10
AMSAT box	1	0	0	0	0	0	0	0	54.84	54.84	0
TMTC redundant	3	0	0	0	0	0	0	0	0	0	0
TMTC antenna +X		0	0	0	0	0	0	0	0	0	0
OBDH	4	30	30	30	30	30	30	30	30	30	30
EPS PEB	4	12	12	12	12	12	12	12	12	12	12
Star Tracker	4	0	0	0	0	0	4.8	0	0	0	0
TMTC antenna -X		0	0	0	0	0	0	0	0	0	0
Reaction Wheel	2	0	0	0	0	0	0	3.3	0	0	0
UCAM	2	0	0	3.6	3.6	0	0	0	0	0	0
Magneto-Torquer +Y	2	2.16	2.16	0	0	0	2.16	2.16	2.16	2.16	0
TMTC Antenna +Y		0	0	0	0	0	0	0	0	0	0
Reaction Wheel 1	5	6	6	14.4	14.4	8.4	6	6	6	6	14.4

Reaction Wheel 2	**5**	**6**	**6**	**14.4**	14.4	**8.4**	**6**	**6**	**6**	**6**	**14.4**
Reaction Wheel 3	**5**	**6**	**6**	**14.4**	14.4	**8.4**	**6**	**6**	**6**	**6**	**14.4**
Reaction Wheel 4	**5**	**6**	**6**	**14.4**	14.4	**8.4**	**6**	**6**	**6**	**6**	**14.4**
Magneto-Torquer-Y	**5**	**2.16**	**2.16**	**0**	0	**0**	**2.16**	**2.16**	**2.16**	**2.16**	**0**
TriTel-S	**3**	**0**	**0**	**0**	0	**8.4**	**0**	**0**	**0**	**0**	**0**
TMTC Antenna +Y		**0**	**0**	**0**	0	**0**	**0**	**0**	**0**	**0**	**0**
TMTC box	**6**	**12**	**33.6**	**12**	33.6	**12**	**12**	**12**	**12**	**33.6**	**12**
Gyro box	**1**	**13.2**	**13.2**	**13.2**	13.2	**13.2**	**13.2**	**13.2**	**13.2**	**13.2**	**13.2**
Magnetometer 1	**3**	**1.44**	**1.44**	**1.44**	1.44	**1.44**	**1.44**	**1.44**	**1.44**	**1.44**	**1.44**
Magnetometer 2	**3**	**1.44**	**1.44**	**1.44**	1.44	**1.44**	**1.44**	**1.44**	**1.44**	**1.44**	**1.44**
TMTC Antenna +Z		**0**	**0**	**0**	0	**0**	**0**	**0**	**0**	**0**	**0**
EPS Battery	**6**	**0**	**0**	**0**	0	**0**	**0**	**0**	**0**	**0**	**0**
LMP	**3**	**0**	**0**	**0**	0	**6**	**0**	**0**	**0**	**0**	**0**
Magneto-Torquer-Z	**6**	**2.16**	**2.16**	**0**	0	**0**	**2.16**	**2.16**	**2.16**	**2.16**	**0**
TMTC antenna -Z		**0**	**0**	**0**	0	**0**	**0**	**0**	**0**	**0**	**0**
total heat dissipation		**100.56**	**122.16**	**131.28**	152.88	**118.08**	**105.36**	**103.86**	**155.4**	**177**	**127.68**

3. THERMAL CONTROL MODELING

3.1 Thermal Desktop software

This analysis is carried on Thermal Desktop (TD) software, which is capable of either finite difference or finite element investigations [26] with/without graphical interfaces. These graphical interfaces include a nongeometric sketchpad-style Sinaps and the geometry-based Thermal Desktop with its companion modules RadCAD and FloCAD [27]. Fig. 2 shows the Thermal Desktop flow chart modeling steps.

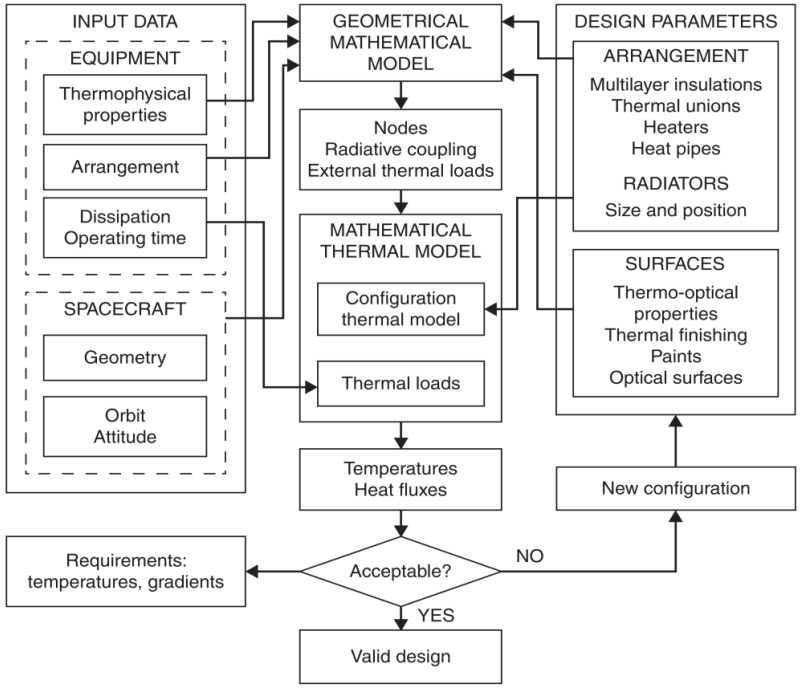

Fig. 2 Thermal Desktop modeling flow chart [28]

The Thermal desktop software divides the simulation modeling into two main tasks to analyze the design and to determine the temperatures. These tasks are geometrical mathematical models and thermal mathematical models. To create the geometrical mathematical model the following parameters are defined: The satellite geometry, components arrangement, thermo-physical properties, the optical properties, and TCS elements arrangement. To create the thermal model the following parameters are defined: Modes of operation (the durations of equipment in operation and the dissipated heat during these periods), satellite orbit, and attitude (Sun and nadir). The selection of the TCS is an iterative process and continuously adjusted by the thermal fillers, insulating systems, radiators, and optical properties until all the temperature requirements are met. The simulation model is used to predict the temperatures that the satellite components will experience. The satellite component temperatures are then compared to the temperature limits. For a component whose temperatures do not comply with its limits, the heat exchanges may be examined to determine the heat sources that cause the problem. Also, the problem may be fixed by applying different TCS passive elements.

3.2 Geometry Creation and Methodology

The model is made by discretizing the satellite into different sections or surfaces, called nodes, where each surface is isothermal, and the satellite is represented as a conductance/capacitance network. The first step in model creation is defining the external geometry. The spacecraft geometry consists of a cuboid structure (six structure panels) and three solar panels (one fixed and two deployable panels). Each external solar or structural panel was created in the thermal desktop software by a rectangle. From structure designers, the external panels are designed of two different materials: honeycomb and aluminum 2024. Aluminum was used for panels number one, four, and five (in the directions +X, -X, and –Y, respectively). For design reasons, the aluminum panels have a thickness of 20.6 mm. Honeycomb panels were used for panels number two, three, and six (in the directions +Y, +Z, and -Z respectively) and the three solar panels. The body or equipment panels have a shell thickness of 0.3 mm and a core thickness of 20 mm with a total thickness of 20.6 mm. The solar panels have a shell thickness of 0.3 mm and a core thickness of 13 mm with a total thickness of 13.6 mm.

The second step is defining the internal geometry that represents the equipment. To create a thermal model of the internal equipment in the Thermal Desktop, all equipment were represented as cylindrical or box shapes. Each piece of equipment has a thickness of 5 mm, heat capacity of Cp =921 J/kg.K, and thermal conductivity of k = 155 W/m.K which approximates all equipment to aluminum[21]. Fig. 3 shows the final view of the ESEO spacecraft geometry in the Thermal Desktop.

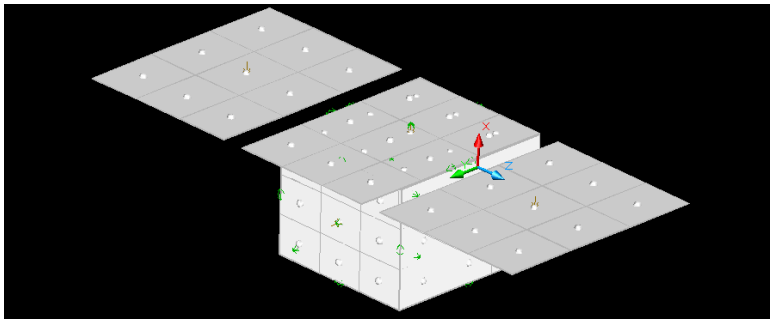

Fig. 3 Screenshot of ESEO model geometry in Thermal Desktop

Nine nodes were defined for each panel, coming to a total of 81 nodes for the external structural and solar panels. Six nodes were defined for each internal equipment to create a total of 126

nodes and the Multi-Layer Insulation (MLI) was modeled as 36 nodes. The numerical model has a whole of 243 nodes. Three types of nodes can be identified in the model: diffusion, arithmetic, and boundary nodes. The satellite is represented by 207 diffusion nodes and 36 arithmetic ones. Some experience is needed to determine the suitable number of nodes for each element (grid sensitivity analysis). In general, more nodes lead to higher resolution in the results. At the same time, increasing the number of nodes will increase the complication of the model and the time needed to build and run the model. Once a well-defined model is settled and initial conditions are specified, steady-state and transient computations can be obtained for all nodes over the chosen time interval.

3.3 Thermal Energy Balance

The thermal modeling is based on a nodal or lumped parameter method. In this method, the satellite is divided into several regions, assumed isothermal, which are called nodes. These nodes exchange heat among each other by conduction and radiation. The external nodes exchange heat with the surroundings via radiation. The temperature of each node is the result of these interactions. TCS in orbit is accomplished by balancing between the absorbed heat from the environment, internal heat generated to the emitted heat by the satellite to space, and energy stored. This thermal energy balance is given by Equation (1) [29]

$$m_i C_i \frac{dT_i}{dt} = Q_{external,i} + Q_{dissipated,i} - Q_{emitted,i} - Q_{conductive,ij} - Q_{radiative,ij} \quad (1)$$

where: $m_i C_i$ the thermal mass; $\left[\frac{\mathrm{J}}{\mathrm{K}}\right]$, $Q_{dissipated,i}$ is the total heat dissipated by the satellite equipment [W], calculated by summation of the operating components heat dissipated during the considered mission as shown in Table 5; $Q_{emitted,i}$ is the heat emitted from the satellite [W] (given by Equation (2))

$$Q_{emitted,i} = \sigma \varepsilon_i A_{radiator,i} T_i^4 \quad (2)$$

where σ Stefan-Boltzmann constant [W/m²K⁴]; $A_{radiator,i}$ the available radiator area; ε_i surface emissivity; $Q_{external,i}$ is external heat fluxes experienced in LEO, given by Equation (3).

$$Q_{external,i} = Q_{solar} + Q_{Albedo} + Q_{Planetary} \quad (3)$$

$Q_{emitted,i}$ the conductive; $Q_{conductive,ij}$ and radiative, $Q_{radiative,ij}$ heat exchange between nodes is given by equations (4), (5) respectively [30].

$$Q_{conductive,ij} = \sum_{j=1}^{n} K_{ij}\left(T_i - T_j\right) \quad (4)$$

$$Q_{radiative,ij} = \sum_{j=1}^{n} R_{ij}\left(T_i^4 - T_j^4\right) \quad (5)$$

The conductive and radiative heat exchange factors are defined as:

$$K_{i,j} = \frac{-kA_i}{dx} \quad (6)$$

$$R_{ij} = A_i F_{ij} \varepsilon_{ij} \quad (7)$$

where: K_{ij} conductive heat exchange factor between nodes i and j [W/K]; R_{ij} radiative heat exchange factor between nodes i and j [W/K^4]; A_i the nodal area [m^2]; dx the distance between two adjacent nodes [m]; F_{ij} the view factor between nodes i and j; ε_{ij} the emissivity between nodes i and j; T_i and T_j the temperatures of nodes i and j, respectively [K].
Then, Equation (1) becomes:

$$m_i C_i \frac{dT_i}{dt} = Q_{external,i} + Q_{dissipated,i} - \sigma \varepsilon_i A_{space,i} T_i^4 - \sum_{j=1}^{n} K_{ij}(T_i - T_j) - \sum_{j=1}^{n} R_{ij}(T_i^4 - T_j^4) \quad (8)$$

3.4 Boundary and operating Conditions

The external fluxes that encounter a satellite are solar, albedo, and planet Infra-Red (IR). Solar flux varies throughout the year because of the varying distance between the earth and Sun because of the eccentricity Earth's orbit. It is assumed that the solar flux is 1371 W/m^2 as a mean value in our study. The rate of solar energy reflected from the Earth is called "albedo". The albedo factor, AF, is the reflected solar radiation from the Earth. AF can vary from 0.18 to 0.55 according to satellite orientation and orbital parameters and is chosen as 0.3 [31]. The absorbed solar radiation by the Earth is reemitted as a long-wave, called IR radiation [32]. The IR energy radiated by the Earth can be changed with season, latitude, the local, and the covering clouds. For most practical purposes, it is assumed that the Earth radiates IR with a constant intensity of 237 W/m^2 [3].
The internal components consume electrical power which is converted to heat. The entire internal heat dissipation in this stage for spacecraft equipment is 155.28 W. Table 5 shows dissipated heat for each piece of equipment in Watts. The operating temperature limits of satellite components are usually determined by the manufacturer as given in Table 6.

Table 6. Operating temperature ranges for satellite elements

Component	T_{min} [ºC]	T_{max} [ºC]	Ref.
Main structure	-40	+85	[20]
Solar cells	-100	+100	[20]
Electronics	-20	+60	[33]
Battery	-20	+40	[34]

The thermo-physical properties for structural panels, solar panels, and internal equipment are defined in Table A1, Table A2, and Table A3 respectively. The optical properties of the internal satellite components and inner faces of structural panels were chosen to have the surface finish of polished aluminum with an emissivity of 0.05 and absorptivity of 0.15 [31]. While the external optical properties were selected as presented in Table 7.

Table 7. External optical properties

Material	Panel	Type	α	ε	Ref.
MLI	Panels 1, 3, 4, 6	Insulation	0.55	0.78	[21]
Aeroglaze A276 white paint	Panel 2	Coating	0.26	0.88	[3]
Teflon Aluminized 1 mm	Panel 5	Radiator	0.14	0.6	[17]
Silver Teflon	Solar panels frontside	Tape	0.08	0.78	[21]
Solar cells	Solar panels frontside	Cells	0.92	0.85	[21]
AMJ-750-LSBU	Solar panels backside	Coating	0.76	0.81	[21]

Once the thermal control temperature limits have been determined, margins must be applied to these limits. A margin of 5°C was applied to both upper and lower temperature limits. This 5°C margin is commonly used by many aerospace companies [15].

4. RESULTS AND DISCUSSIONS

4.1 Thermal Desktop Results for Operational Phase

Fig. 4 shows the temperature variation for the operational phase (28 orbits) as predicted by Thermal Desktop. The results show that all equipment normally operate within specified limits. Regarding the structural panels of the satellite shown in Fig. 4 (b), there are three typically noticeable parts.

First is panel 2 which is the top panel, that receives only the solar flux. Panel 5 (bottom panel) is affected by the albedo and the infrared radiation of Earth. The third one is the remaining sides which are almost the same.

The different materials used in the manufacturing of panels 2, panel 5, and panels 1,3,4, and 6 with their different thermal properties are chosen such that all structural panels cope with their temperature limits. The predicted AMSAT and Gyro temperatures for the operational phase analyses are depicted in Fig. 4(c). It is noted that the gyro mean temperature variation is higher than AMSAT mean temperature variation because the gyro is continuously operated while AMSAT is switched on only in orbits 5, 7, 20, and 28. The Gyro temperature levels at 19.1°C as maximum and 8.22°C as minimum temperature and AMSAT temperature levels at 19.83°C as maximum and 4.49°C as the minimum temperature.

The repeated oscillation in the temperature is due to the orbital variation of entering and leaving the Earth's shadow. The jump in temperature for AMSAT is due to the change in the satellite orientation (nadir orientation in orbits 4, 8, 19, and 27) for shooting and the increase of internal heat dissipation of this equipment by 55.84 W in orbits 5, 7, 20, and 28. Table 8 summarizes results for operational phase maximum and minimum temperatures for all satellite elements obtained from Thermal Desktop. A margin of 5°C was applied to both upper and lower temperatures and the results are compared to the operating limits. As the table shows, all the temperature requirements are met, for all the satellite components by using passive TCS.

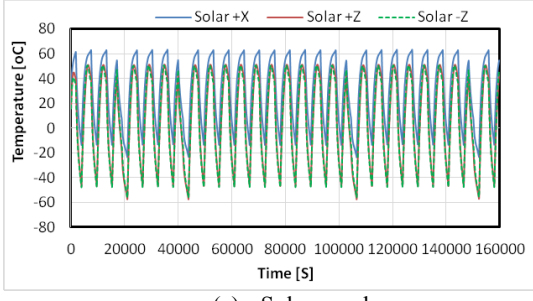

(a) Solar panels

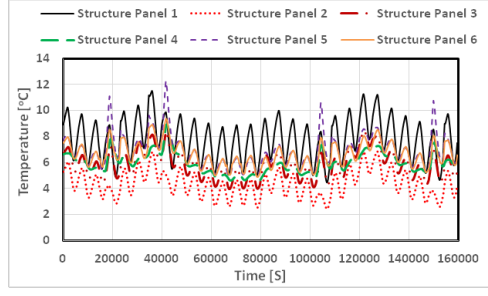

(b) Structure panels

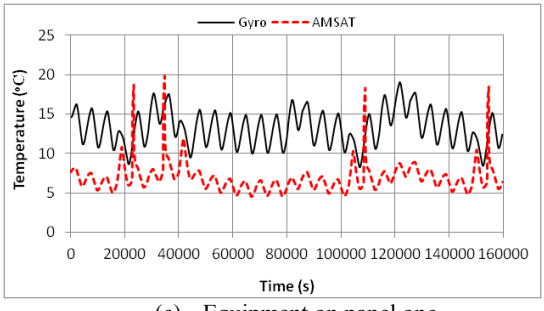

(c) Equipment on panel one

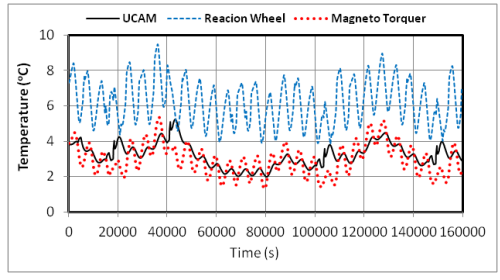

(d) Equipment on panel two

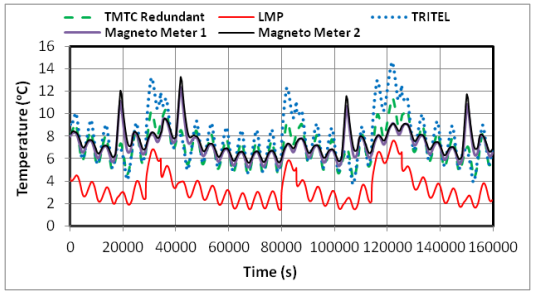

(e) Equipment on panel three

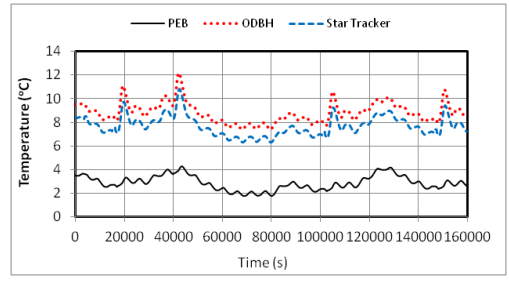

(f) Equipment on panel four

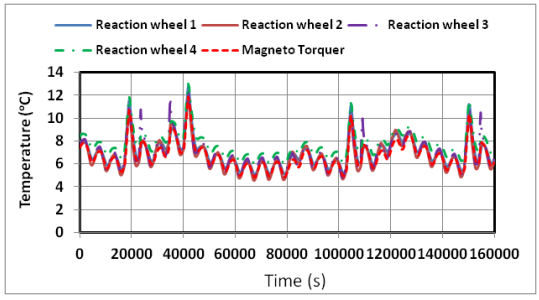

(g) Equipment on panel five

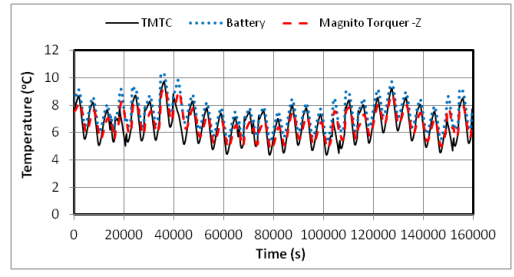

(h) Equipment on panel six

Fig. 4 Temperature variation for satellite panels and internal components in operational phase (28 orbits) as predicted by Thermal Desktop.

Table 8. Summary of Thermal Desktop results for the operational phase.

Component	Predicted Temperature		Margin	Predicted Temperature with margin		Operating Limit	
	Max	Min		Max	Min	Max	Min
Solar panel +X	63.24	-23.35	5	68.24	-28.35	-100	+100
Solar Panel +Z	51.17	-57.77	5	56.17	-62.77	-100	+100
Solar panel -Z	50.77	-56.35	5	55.77	-61.35	-100	+100
Panel 1	11.52	4.49	5	16.52	-0.51	-40	+85
Panel 2	6.85	2.43	5	11.85	-2.57	-40	+85
Panel 3	8.47	3.98	5	13.47	-1.02	-40	+85
Panel 4	8.95	4.63	5	13.95	-0.37	-40	+85
Panel 5	12.27	5.03	5	17.27	0.03	-40	+85
Panel 6	9.36	4.87	5	14.36	-0.13	-40	+85
Gyro box	19.1	8.22	5	24.1	3.22	-20	+60
AMSAT box	19.83	4.49	5	24.83	-0.51	-20	+60
UCAM	5.2	2	5	10.2	-3	-20	+60
Reaction Wheel +Y	9.47	3.82	5	14.47	-1.18	-20	+60
Magneto-Torquer +Y	5.35	1.37	5	10.35	-3.63	-20	+60
TMTC redundant	11.42	4.18	5	16.42	-0.82	-20	+60
LMP	7.65	1.46	5	12.65	-3.54	-20	+60
TRITEL S	14.64	3.7	5	19.64	-1.3	-20	+60
Magnetometer 1	12.36	5.2	5	17.36	0.2	-20	+60
Magnetometer 2	13.3	5.6	5	18.3	0.6	-20	+60
EPS PEB	4.3	1.8	5	9.3	-3.2	-20	+60
OBDH	12.21	7.37	5	17.21	2.37	-20	+60
Star Tracker	10.8	6.28	5	15.8	1.28	-20	+60
Reaction Wheel 1	12.75	5.05	5	17.75	0.05	-20	+60
Reaction Wheel 2	11.89	4.56	5	16.89	-0.44	-20	+60
Reaction Wheel 3	12.28	4.79	5	17.28	-0.21	-20	+60

Component	Predicted Temperature		Margin	Predicted Temperature with margin		Operating Limit	
	Max	Min		Max	Min	Max	Min
Reaction Wheel 4	11.86	5.92	5	16.86	0.92	-20	+60
Magneto-Torquer-Y	11.86	4.82	5	16.86	-0.18	-20	+60
TMTC box	9.74	4.36	5	14.74	-0.64	-20	+60
EPS Battery	10.3	5.3	5	15.3	0.3	-20	+40
Magneto-Torquer-Z	9.27	4.8	5	14.27	-0.2	-20	+60

4.2 Operational Phase Comparative Results

The final thermal design of the ESEO satellite introduced in [21] contains both passive and active thermal control systems. The components that didn't satisfy their temperature ranges were the Electric Power System control unit (EPS-PEB), Telemetry and Telecommand system (TMTC), magnetometers, EPS battery, reaction wheel 1-4, Onboard Data Handling system (OBDH), and TriTel-S. The reduced temperature was eliminated by using an electric heater. In this section, the major task is to compare the Thermal Desktop results after using passive TCS with ESEO published results by ESATAN software [21]. Fig. 5 and Table 9 show comparisons between the two software packages of most satellite internal components for the operational phase only. The ESATAN results show that most equipment temperatures are out of range or very close to the lower limit, except the Gyro, while Thermal Desktop results lie within suitable margins as mentioned previously. For example, the predicted battery temperature for the operational phase analyses is displayed in Fig. 5(a). The red line is the results found by thermal Desktop, showing that the battery temperature levels at 10.3°C as maximum and 5.3°C as the minimum temperature. It also shows that the battery temperature predicted by the ESATAN analysis (purple line) is -7°C and -18°C as maximum and minimum temperatures, respectively. This temperature range is very close to the battery lower margin (-20°C). This comparison indicates that the ESATAN results concerning the battery must be supported by an electric heater as an active thermal control element to raise its temperature to a suitable margin. The Thermal Desktop model results show no need for active thermal control.

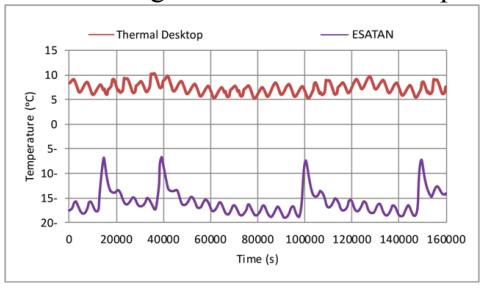

(a) Battery

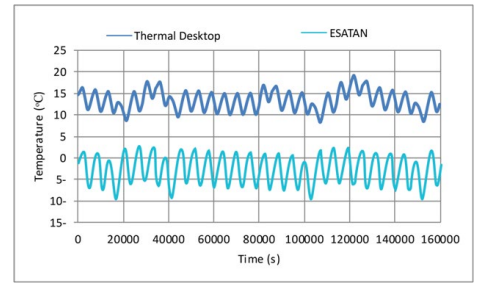

(b) Gyro

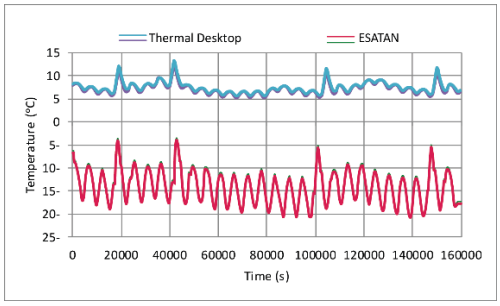

(c) Magneto meter 1and 2

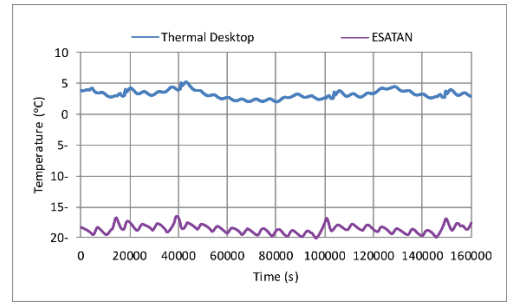

(d) uCAM

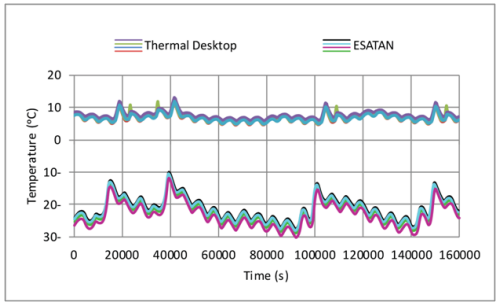

(e) Reaction wheel 1-4

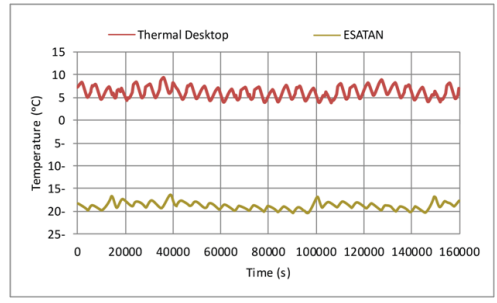

(f) Reaction wheel +Y

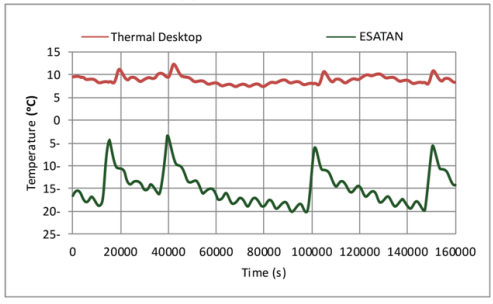

(g) OBDH

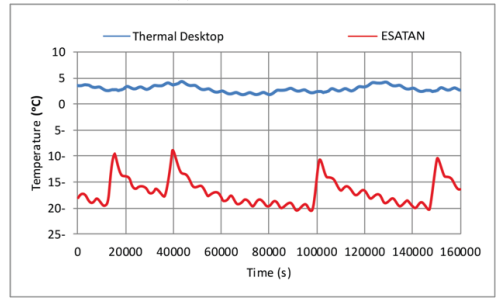

(h) Equipment on panel six

Fig. 5 Satellite internal components temperature variation for operational phase as predicted by Thermal Desktop and ESATAN

Table 9. Summary of comparative results for operational phase obtained from both Thermal Desktop and ESATAN

Component	Operating Limits		Thermal Desktop Results		ESATAN Results	
	Max	Min	Max	Min	Max	Min
Battery	40	-20	10.3	5.3	-6	-18
Gyro	40	-20	19.1	8.22	3	-10
Magnetometer 1	40	-20	12.36	5.2	-4	-22
Magnetometer 2	40	-20	13.3	5.6	-4	-22
uCAM	40	-20	5.2	2	-17	-20
Reaction Wheel 1	40	-20	12.75	5.05	-7	-23
Reaction Wheel 2	40	-20	11.89	4.56	-7	-23
Reaction Wheel 3	40	-20	12.28	4.79	-7	-23
Reaction Wheel 4	40	-20	11.86	5.92	-7	-23
Reaction Wheel +Y	40	-20	9.47	3.82	-15	-21
OBDH	40	-20	12.21	7.37	-6	-17
PEB	40	-20	4.3	1.8	-11	-18

5. CONCLUSIONS

In this paper, a passive thermal control design and analysis were carried out for the ESEO satellite. The thermal model was created in Thermal Desktop software. The model was run for the operative phase which includes cycles of 28 orbits with 10 modes. The satellite thermal design is an iterative process and the model is subsequently modified to improve the thermal performance of the spacecraft. Equipment distribution, emissivity, absorptivity, and MLI placement are the main parameters that can be varied to change the temperature distribution. Orbital parameters are really important in thermal analysis. The temperature results obtained from simulation were presented and compared with ESEO published results by ESATAN

software to show that the passive thermal control system meets the temperature requirements. The battery temperatures which are considered as one of the key drivers of the thermal design remain within the specified temperature limits (5.3ºC to 10.3ºC) for the operative phase. It has a narrower allowable temperature range (-20ºC to 40ºC). The results showed that the passive thermal control system was able to meet the requirements and maintain the component temperatures and panels within their design limits. From this study, we come to the specific conclusion that the results have shown similarities with other related-type satellites and with the theory explained (passive thermal control type).

REFERENCES

[1] S. Corpino, M. Caldera, F. Nichele, M. Masoero, N. Viola, Thermal design and analysis of a nanosatellite in low earth orbit, *Acta Astronaut.*, **115**:247–261, 2015, https://doi.org/10.1016/j.actaastro.2015.05.012.

[2] A. Torres, D. Mishkinis, T. Kaya, Mathematical modeling of a new satellite thermal architecture system connecting the east and west radiator panels and flight performance prediction, *Appl Therm Eng*; **65**:623–632, 2014, https://doi.org/10.1016/j.applthermaleng.2013.11.040.

[3] P. Fortescue, J. Stark, G. Swinerd, editors, Systems Engineering Spacecraft Systems, Third Edit. Rh-Er Sireet, Hoboken., NJ 07030, USA: John Wiley It Sons Inc., 2003.

[4] M. Bonnici, P. Mollicone, M. Fenech, M. Anthony, Analytical and numerical models for thermal related design of a new pico- satellite, *Appl. Therm. Eng*. **159**:113908, 2019. https://doi.org/10.1016/j.applthermaleng.2019.113908.

[5] J. M. Elliott, *The thermal design and analysis of the CanX-4/-5 and NEMO-AM nanosatellites*, MSc Thesis 2014.

[6] R. Kovács, V. Józsa, Thermal analysis of the SMOG-1 PocketQube satellite, *Appl Therm Eng*, 2018, https://doi.org/10.1016/j.applthermaleng.2018.05.020.

[7] E. Escobar, M. Diaz, J. C. Zagal, Evolutionary design of a satellite thermal control system: Real experiments for a CubeSat mission, *Appl Therm Eng*, **105**:490–500, 2016, https://doi.org/10.1016/j.applthermaleng.2016.03.024.

[8] M. Donabedian, *Spacecraft Thermal Control Handbook*, Volume **II**: Cryogenics. vol. **I**, 2004, https://doi.org/10.2514/4.989148.

[9] J. Gaite, G. Fernández-Rico, Linear approach to the orbiting spacecraft thermal problem, *J Thermophys Heat Transf.*, **26**:511–22, 2012, https://doi.org/10.2514/1.T3748.

[10] S. Czernik, *Design of the Thermal Control System for Compass-1e*, University of Applied Sciences Aachen, 2004.

[11] D. Q. Dinh, *Thermal Modeling of Nanosat*, San José State University, 2012.

[12] S. Jos, *Thermal Modeling of Nanosat*, MSc Thesis 2012.

[13] M. M. Garzon, *Development and Analysis of thermal Design for the OSIRIS-3U Cubesat*, The Pennsylvania State University, 2012.

[14] M. R. Ali, *Design and Implementation of Ground Support Equipment for Characterizing the Performance of XPOD and CNAPS & Thermal Analysis of CNAPS Pressure Regulator Valve. University of Toronto*, 2009.

[15] E. Verheire, *Thermal analysis of the QARMAN re-entry satellite*, von Karman Institute for Fluid Dynamics, 2015.

[16] T. Van. Boxtel, *Thermal modelling and design of the DelFFi satellites*, Delft University of Technology, 2015.

[17] K. E. Boushon, T*hermal analysis and control of small satellites in low Earth orbit*, Missouri University of Science and Technology, 2018.

[18] J. R. Kopacz, R. Herschitz, J. Roney, Small satellites an overview and assessment, Acta Astronautica *2020*, **170**:93–105, https://doi.org/10.1016/j.actaastro.2020.01.034.

[19] F. J. Fuenmayora, V. Alcayde, A. Vercher-Martíneza, Thermal control of a spacecraft: Backward-implicit scheme programming and coating materials analysis, *Adv Sp Res*, 2021, **68**:1975–88, https://doi.org/https://doi.org/10.1016/j.asr.2021.03.041.

[20] L. Jacques, *Thermal Design of the Oufti-1 nanosatellite*, University of Liège, 2008.

[21] M. J.-L. C. Poucet, *Phase-B Thermal Control Subsytem Design for the ESEO Satellite*, Politecnico di Milano, 2012.

[22] D. Felipe, I. Muraoka, E. C. Garcia, Thermal Control Design Conception of the Amazonia-1 Satellite, *J Aerosp Technol Manag São José Dos Campos*, 2014, **6**:169–76, https://doi.org/10.5028/jatm.v6i2.320.

[23] B. S. Cotton, *Design, Analysis, Implementation and Testing of the Thermal Control, and Attitude*

Determination and Control Systems for the Canx-7 Nanosatellite Mission, University of Toronto, 2014.
[24] S. Chandrashekar, *Thermal Analysis and Control of MIST CubeSat*, KTH Royal Institute Of Technology, 2016.
[25] D. P. Bell, T. D. Panczak, B. A. Cullimore, *Thermal Desktop® Advanced Modeling Guide*, Cullimore and Ring Technologies, Inc.; 2017.
[26] M. Bulut, N. Sozbir, Analytical investigation of a nanosatellite panel surface temperatures for different altitudes and panel combinations, *Appl Therm Eng*, 2015, **75**:1076–83, https://doi.org/10.1016/j.applthermaleng.2014.10.059.
[27] B. A. Cullimore, S. G. Ring, D. A. Johnson, *SINDA/FLUINT General Purpose Thermal/Fluid Network Analyzer User's Manual*, C&R Technologies, Inc. ("CRTech"), 2015.
[28] J. Meseguer, I. Pérez-Grande and A. Sanz-Andrés, Spacecraft thermal control, Woodhead Publishing Limited, Sawston, Cambridge, UK. First Edd. 2012.
[29] R. Karam, *Satellite Thermal Control for Systems Engineers*, 1998, https://doi.org/10.2514/4.866524.
[30] B. Anderson, C. Justus, G. Batts, Guidelines for the selection of near-earth thermal environment parameters for spacecraft design, *Nasa TM-2001-211221*, 2001:32.
[31] C. B. Van Outryve, A Thermal Analysis and Design Tool for Small Spacecraft, San Jose State University, 2008.
[32] D. G. Gilmore, Spacecraft thermal control handbook, Volume 1: Fundamental Technologies, The Aerospace Press, E1 Segundo, California, Second Edd., 2002.
[33] M. Day, 30 Years of Commercial Components In Space: Selection Techniques Without Formal Qualification, 13th Annu. AIAA/USU Conf. Small Satell. SSC99-IIA-2, 1999, p. 1–8.
[34] * * * *B ST BAT-100, Berlin Sp Technol 2020*, https://www.berlin-space-tech.com/wp-content/uploads/2020/07/PFR-PR10-Battery-Flyer-V1.00-.pdf (accessed 19 September 2020).

NOMENCLATURE

Abbreviations

ADCS	Attitude determination and control System	LTAN	Local time of ascending node
ESA	European Space Agency	MLI	Multi-Layer Insulation
ESEO	European Student Earth Orbiter	MTC	Military Technical College
FDM	Finite Difference Method	NASA	National Aeronautics and Space
FEM	Finite Element Method	SFL	Space Flight Laboratory
IR	Infra-Red	STC	Space Technoloy Center
LET	Linear Energy Transfer	TCS	Thermal Control Subsystem
LEO	Low Earth Orbit	WCC	Worst-Case Cold
LMP	Langmuir plasma diagnostic probe	WCH	Worst-Case Hot

Symbols

A_i	Nodal area [m^2]
dx	The distance between two adjacent nodes
F_{ij}	The view factor between nodes i and j
k	The thermal conductivity of the material
K_{ij}	conductive heat exchange factor between nodes i and j [W/K]
$m_i C_i$	Thermal mass of node I [J/K]
Q	Amount of heat transferred rate [W]
R_{ij}	Radiative heat exchange factor between nodes i and j [W/K^4]
T	Temperature [^oC or K]
t	Time [s or hr]
α	Absorptivity
ε	Emissivity
σ	Stefan-Boltzmann constant [W/m^2K^4]

APPENDICES

Table A.1 External panel Thermo-physical properties

Panel No.	Material	Density [kg/m^3]	Specific heat C_p [J/kg K]	Conductivity [W/m K]
Panel 1	Aluminum	522.878	921	155
Panel 2	Honeycomb	725.701	921	97.857
Panel 3	Honeycomb	791.074	921	97.857
Panel 4	Aluminum	541.292	921	155
Panel 5	Aluminum	1177.37	921	155
Panel 6	Honeycomb	707.123	921	97.857

Table A.2 Solar panels Thermo-physical properties

Solar data	Material	Density [kg/m^3]	C_p [j /kg K]	Conductivity [W/m K]
Solar +X	Honeycomb	503.953	921	97.85714
Solar -Z	Honeycomb	503.953	921	97.85714
Solar +Z	Honeycomb	503.953	921	97.85714

Table A.3 Internal equipment thermo-physical properties

Component	Shape	Mass [kg]	Volume $\times 10^{-6}$[m^3]	Density [kg/m^3]
AMSAT box	Box	0.72	695	1035.98
TMTC redundant	Box	4.61	836	5514.35
TMTC antenna +X	Box	0.12	198.12	605.69
OBDH	Box	12	1445.31	8302.72
EPS PEB	Box	8.4	1491.5	5631.91
Star Tracker	Box	2.06	341.472	6032.7
TMTC antenna -X	Box	0.12	198.12	605.69
Reaction Wheel	Box	0.96	2617.25	366.8
UCAM	Box	0.72	222.405	3237.34
Magneto- Torquer +Y	cylinder	1.44	12.4056	11607.66
TMTC Antenna +Y	Box	0.12	198.12	605.69
Reaction Wheel 1	Box	1.8	977.75	1840.96
Reaction Wheel 2	Box	1.8	977.75	1840.96
Reaction Wheel 3	Box	1.8	977.75	1840.96
Reaction Wheel 4	Box	1.8	977.75	1840.96
Magneto- Torquer -Y	cylinder	1.44	12.4056	11607.66
Tri-Tel S	Box	1.44	110.39	13044.66
TMTC Antenna +Y	Box	0.12	198.12	605.69
TMTC box	Box	4.61	836	5514.53
Gyro box	Box	1.8	386.32	4659.35
Magnetometer 1	Box	0.07	727.5	962.2
Magnetometer 2	Box	0.07	727.5	962.2
TMTC Antenna +Z	Box	0.12	198.12	605.69
EPS Battery	Box	7.98	6035	1322.29
LMP	cube	0.96	192	5000
Magneto - Torquer -Z	cylinder	1.44	12.4056	11607.66
TMTC antenna -Z	Box	0.12	198.12	605.69